UDC 621.3 https://doi.org/10.20998/2074-272X.2024.1.01

K. Latreche, R. Taleb, A. Bentaallah, A.E. Toubal Maamar, M. Helaimi, F. Chabni

# Design and experimental implementation of voltage control scheme using the coefficient diagram method based PID controller for two-level boost converter with photovoltaic system

***Introduction.*** *Currently, in the solar energy systems and a variety of electrical applications, the power converters are essential part. The main challenge for similar systems is controller design. In the literature, the PID controller has proved its effectiveness in many industrial applications, but determining its parameters remains one of the challenges in control theory field. The* ***novelty*** *of the work resides in the design and experimental implementation of a two-level boost DC-DC converter controlled by a PID controller for photovoltaic (PV) maximum power extraction.* ***Purpose.*** *Analysis and control of the two-level boost topology with renewable energy source and design of the PID controller parameters using simple and accurate method.* ***Methods.*** *PID coefficients are optimized using Coefficient Diagram Method (CDM) in the MATLAB environment.* ***Results.*** *A mathematical model of a two-level boost converter with PID controller and PV energy source was developed and analyzed. The model allows to design the controller parameters of the proposed system.* ***Practical value.*** *A prototype steered by the proposed CDM-PID controller was tested using an Arduino embedded board. A comparison between the simulation results and the experimental one is presented. The obtained results illustrate that the experimental results match the simulation closely, and the proposed CDM-PID controller provides a fast and precise results.* References 24, table 2, figures 16.

*Key words:* **power electronics, energy conversion, two-level boost converter, coefficient diagram method controller.**

***Вступ***. *В даний час перетворювачі потужності є невід'ємною частиною сонячних енергетичних систем та різних електричних пристроїв. Основною проблемою для таких систем є проектування контролера. У літературі ПІД-регулятор довів свою ефективність у багатьох промислових застосуваннях, але визначення його параметрів залишається однією з проблем у галузі теорії управління.* ***Новизна*** *роботи полягає у розробці та експериментальній реалізації дворівневого підвищувального перетворювача постійного струму, керованого ПІД-регулятором, для отримання максимальної потужності фотоелектричних пристроїв.* ***Мета***. *Аналіз та управління дворівневою топологією підвищення з використанням відновлюваного джерела енергії та розрахунок параметрів ПІД-регулятора простим та точним методом.* ***Методи***. *Коефіцієнти ПІД оптимізуються за допомогою методу діаграми коефіцієнтів (CDM) у середовищі MATLAB.* ***Отримані результати***. *Розроблено та проаналізовано математичну модель дворівневого підвищувального перетворювача з ПІД-регулятором та фотоелектричним джерелом енергії. Модель дозволяє спроєктувати параметри контролера пропонованої системи.* ***Практична цінність***. *Прототип, керований пропонованим контролером CDM-PID, протестували з використанням вбудованої плати Arduino. Наведено порівняння результатів моделювання з експериментальними даними. Отримані результати показують, що експериментальні результати близько відповідають моделюванню, а пропонований CDM-ПІД-регулятор забезпечує швидкі та точні результати.* Бібл. 24, табл. 2, рис. 16.

*Ключові слова:* **силова електроніка, перетворення енергії, дворівневий підвищувальний перетворювач, регулятор методу діаграми коефіцієнтів.**

**Introduction.** Nowadays, solar and wind energies are from the most contributor for power generation among different renewable energy resources. The use of solar energy because of their advantageous such as the free availability, solar energy systems on buildings have minimal impact on the environment, electricity produced by solar cells is clean (not produce air pollution or carbon dioxide) and silent [1-3].

In solar energy systems and a variety of electrical applications, the power converters are essential part. There is a several type of converters: AC to DC converters, DC to AC converters, AC to AC converters, and DC to DC converters. Also, the use of multilevel converters topologies in power circuits has many benefices, including the increase of the voltage level, the reduction of stress across static switches, the improvement of power factor with the reduction of power losses, the reduction of filter size [4-9]. DC to DC converters are widely used in many modern electronic systems. They convert a DC input voltage into a different DC output voltage, and are widely used in power supplies for all types of electronic devices, such as computers, cell phones, tablets and telecommunications equipment.

An overview of DC-DC converters allows us to conclude the importance of this type of converter. Authors in [10] have presented enhanced fuzzy logic controller using boost DC-DC converter topologies for a grid system. In the work [11] have proposed high step up boost converter for uninterrupted power supply using renewable energy resources (wind and photovoltaic (PV)). Authors in [12] have discussed switching DC step-up/step-down regulators voltage for maximum power transmission. In the work [13] have presented DC-DC converter topologies for energy management system. Authors in [14] have proposed five-level inverter alimented by DC-DC converter with artificial intelligence control. The control of DC-DC converters is an important topic in modern electronic circuit design. Precise regulation of the output voltage of a DC-DC converter is crucial to ensure the smooth operation of the overall electronic system. The intelligent control techniques and the PID control method are often used to control these converters [15, 16]. However, optimizing PID coefficients can be difficult, especially for converters with variable frequency switching.

The **goal** of the paper is design and experimental implementation of a two-level boost DC-DC converter controlled by a PID controller for PV maximum power extraction. The PID coefficients are optimized using Coefficient Diagram Method (CDM); hence the Maximum Power Point Tracking (MPPT)-PID controller adopting CDM is utilized for providing better accuracy. A two-level boost DC-DC converter is exploited which boosts the oscillating PV voltage. The two-level boost DC-DC topology, the design of MPPT-PID controller based on CDM, and the main findings are summarized in this article.

**Theoretical background of the CDM.** CDM is an algebraic approach, proposed by Prof. Manabe to design

the controller parameters [17]. The standard block scheme of CDM is shown in Fig. 1, on which $R(s)$ is the reference input signal; $Y(s)$ is the output signal; $d(s)$ is the disturbance; $N(s)$ is the numerator polynomial of the controlled system; $D(s)$ is the denominator polynomial of the controlled system; $A(s)$, $B(s)$, and $F(s)$ are the CDM controller polynomials.

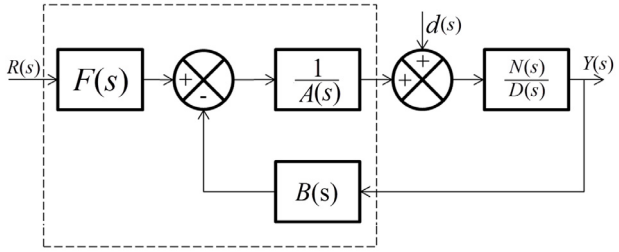


Fig. 1. The standard block diagram of CDM

The closed-loop transfer function of the system can be written as:

$$Y(s)=\frac{N(s)F(s)}{P(s)}R(s)+\frac{A(s)N(s)}{P(s)}d(s), \qquad (1)$$

where $P(s)$ is the characteristic polynomial of the closed-loop system presented as:

$$P(s)=A(s)D(s)+N(s)B(s). \qquad (2)$$

The polynomials $A(s)$ and $B(s)$ of the CDM controller structures are given as:

$$A(s)=\sum_{i=0}^{x} l_i s^i; \quad B(s)=\sum_{i=0}^{y} k_i s^i, \qquad (3)$$

where $x$ and $y$ are the degrees of CDM controller.

Next step of design consists of the calculation of the target polynomial $P_t(s)$ as follows:

$$P_t(s)=a_0\left[\left(\sum_{i=2}^{n}\left(\prod_{j=1}^{i-1}\frac{1}{\gamma_{i-j}^{j}}\right)(\tau s)^i\right)+\tau s+1\right], \qquad (4)$$

where $n$ is the order of the characteristic polynomial $P(s)$; $\tau$ is the equivalent time constant; $\gamma_i$ is the stability indices.

In design of CDM controller, the most important point is setting of key parameters ($\gamma_i$ and $\tau$), because the key parameters come into closely relation with the dynamic system performances (rapidity, robustness, stability). Value of equivalent time constant ($\tau$) has relation with the system rapidity, because it has an impact on the rise time and settling time. Values of stability parameter ($\gamma_i$) have relation with the system stability and robustness, because have impact on the steady state error. According to [17] $\gamma_i$ and $\tau$ values can be selected as follows: $\gamma_i$ values can be written as: {2.5, 2, 2...2}. Usually ($\gamma_i$) is selecting from the range of (1.5 to 4) to have a good stability performance based on Routh-Hurwitz stability criterion and Lipatov's stability criterion. In other hand, the key parameters ($\gamma_i$ and $\tau$) can be adjusted to have good desired performances [17-19].

Last step of design is determination of the PID controller gains. Putting $P(s) = P_t(s)$, then presenting the equations system in matrix form ($AX = B$). Note that $X = [k_2; k_1; k_0; l_1]$ is the vector of gains for estimating the PID controller parameters; $k_p$ is the proportional gain of PID controller; $k_i$ is the integral gain of PID controller; $k_d$ is the derivative gain of PID controller:

$$k_p = k_1/l_1; \quad k_i = k_0/l_1; \quad k_d = k_2/l_1.$$

**Description of the proposed two-level boost connected PV system.** Figure 2 displays the proposed boost-connected PV system. It includes a two-level boost converter linked to PV system.

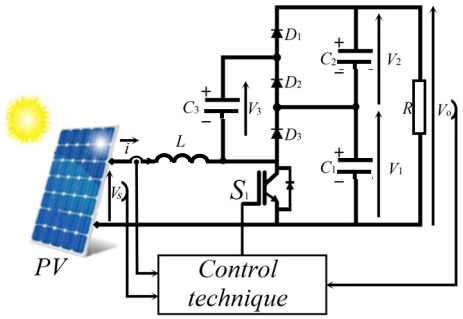


Fig. 2. The proposed boost-connected PV scheme

To study the control of the system, we must present briefly the principle and the mathematical model of each element of the system.

**Model of the PV panel.** In the literature several PV models have been discussed. The models differ from each other in the procedure and the number of parameters involved in the calculation of the current-voltage pair [20-22]. Figure 3 illustrates the most common equivalent electrical circuit of the PV module.

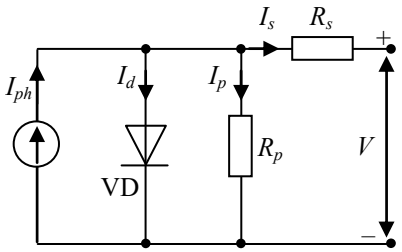


Fig. 3. Equivalent electrical circuit of a PV cell (one diode model)

From the electrical circuit, we can obtain the formula that allows us to obtain the *I-V* characteristic of the PV cell and panel. The law of nodes lets us to write the following relationship (5):

$$I = I_{ph} - I_d - I_p = \\ = I_{ph} - I_s\left(e^{\left(\frac{q(V+R_sI)}{nkT}\right)}-1\right)-\frac{V+R_sI}{R_p}, \qquad (5)$$

where $I$, $V$ are the current and the voltage generated by the solar cell; $I_d$, $I_p$ are the diode current and the parallel resistor current; $R_s$, $R_p$ are the series and parallel resistors of the solar cell; $k$ is the Boltzmann constant ($k = 1.38 \cdot 10^{-23}$ J/K); $n$ is the ideality factor of the solar cell, varies between 1 and 2; $T$ is the temperature of a diode; $q$ is the charge of an electron ($q = 1{,}6 \cdot 10^{-19}$ C); $I_{ph}$ is the photocurrent generated by the solar cell.

The photocurrent $I_{ph}$ is proportional to the solar radiation $E$ and is assumed to be linear as a function of the surface temperature $T$ of the cell, it can be described as:

$$I_{ph}=\frac{E}{E_{ref}}\left(I_{phref}+\mu_{scc}\left(T-T_{ref}\right)\right), \qquad (6)$$

where $E$ is the real solar irradiance, W/m²; $E_{ref}$ is the standard test conditions (STC) irradiance, W/m²; $T$ is the

operating temperature; $T_{ref}$ is the STC temperature; $\mu_{scc}$ is the temperature coefficient of the short-circuit current; STC conditions are cell temperature of 25 °C and global solar irradiance of 1000 W/m².

The choice of the series and parallel resistance values for simulation is detailed in papers [23, 24]. The series and parallel resistance values can be calculated as:

$$R_p > \frac{10V_{co}}{I_{cc}};\ \ R_s < \frac{0.1V_{co}}{I_{cc}}, \tag{7}$$

where:

$$I_{CC} \approx I_{ph};\quad V_{CO} = V_t \ln\left(\frac{I_{ph}}{I_S}+1\right);\quad V_t = \frac{nkT}{q},$$

where $V_t$ is the thermal voltage of the diode; $V_{co}$ is the open circuit voltage; $I_{cc}$ is the short-circuit current.

For a solar panel with $N$ cells, we can write the saturation current as:

$$I_S = \frac{I_{ph}}{e^{\left(\frac{V_{CO}}{N_{cell}\cdot V_t}\right)}-1}. \tag{8}$$

**Model of the two-level boost converter.** Figure 4 displays the topology of the two-level boost converter. A two-level boost converter is typically composed of one switch $S_1$, one inductance $L$, three capacitors $C_1$, $C_2$, $C_3$, three diode $D_1$, $D_2$, $D_3$, one DC power supply or renewable energy source (in our case the DC power supply is replaced by a PV), one resistor $R$ as load. The output voltage $V_0$ is related to the voltage of the two capacitors $V_1$ and $V_2$. Thus, $V_0 = V_1 + V_2 = 2V_c$. The output voltage can be calculated as:

$$V_0 = \frac{2V_s}{1-\alpha}, \tag{9}$$

where $\alpha$ is the duty cycle; $V_s$ is the input voltage.

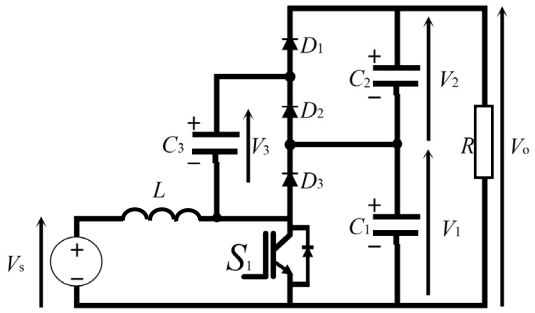

Fig. 4. Topology of the two-level boost converter

The state-space model of the two-level boost converter can be written with the following system of equations:

$$\begin{cases} \dfrac{dI_L}{dt} = -\dfrac{(1-\alpha)}{2\cdot L}\cdot v_0 + \dfrac{1}{L}\cdot v_s; \\ \dfrac{dv_0}{dt} = \dfrac{(1-\alpha)}{C}\cdot I_L + \dfrac{2}{R\cdot C}\cdot v_0. \end{cases} \tag{10}$$

In matrix form, the state space model of the system is given as:

$$\begin{cases} \dot{X} = A\cdot X + B\cdot U; \\ Y = C\cdot X, \end{cases} \tag{11}$$

where:

$$A = \begin{bmatrix} 0 & -\dfrac{(1-\alpha)}{2\cdot L} \\ \dfrac{(1-\alpha)}{C} & -\dfrac{2}{R\cdot C} \end{bmatrix};\quad B = \begin{bmatrix} 1/L \\ 0 \end{bmatrix};\quad C = \begin{bmatrix} 0 & 1 \end{bmatrix}.$$

Based on the state space model, the system transfer function can be expressed using the complement (com) and the determinant (det) of a matrix ($SI_2 - A$), as:

$$G(S) = \frac{C\cdot(\mathrm{com}(SI_2 - A))^T \cdot B}{\det(SI_2 - A)}. \tag{12}$$

By applying some mathematical manipulations, the transfer function of the system is given as:

$$G(S) = \frac{\dfrac{(1-\alpha)}{L\cdot C}}{S^2 + \left(\dfrac{2}{R\cdot C}\right)S + \dfrac{(1-\alpha)^2}{2\cdot L\cdot C}}. \tag{13}$$

**CDM-PID controller design for the proposed system.** To identify the parameters of the proposed controller used in this application by the CDM technique, the open-loop transfer function $G(s)$ of the system is used. First, the transfer function $G(s)$ of the system is given in polynomial forms as follow:

$$\begin{cases} N(s) = \dfrac{(1-\alpha)}{L\cdot C}; \\ D(s) = S^2 + \left(\dfrac{2}{R\cdot C}\right)S + \dfrac{(1-\alpha)^2}{2\cdot L\cdot C}. \end{cases} \tag{14}$$

In this work, we have chosen a second-order polynomial controller $C(s)$ given by the following structure:

$$\begin{cases} B(s) = k_2 s^2 + k_1 s^1 + k_0; \\ A(s) = l_2 s^2 + l_1 s^1 + l_0. \end{cases} \tag{15}$$

So, the transfer function $C(s)$ of the controller is given by:

$$C(s) = \frac{k_2 s^2 + k_1 s^1 + k_0}{l_2 s^2 + l_1 s^1 + l_0}. \tag{16}$$

The characteristic expression of the standard PID controller is written as:

$$C_{PID}(s) = k_p + \frac{k_i}{S} + k_d S = \frac{k_p S + k_i + k_d S^2}{S}. \tag{17}$$

By identification between (16) and (17), the second-order polynomial controller is written as:

$$C(s) = \frac{k_2 s^2 + k_1 s^1 + k_0}{l_1 s^1} = \frac{k_2}{l_1} S + \frac{k_1}{l_1} + \frac{k_0}{l_1 S}. \tag{18}$$

By identification between (17) and (18), the PID controller parameters can be estimated as:

$$k_p = k_1/l_1;\quad k_i = k_0/l_1;\quad k_d = k_2/l_1.$$

The characteristic polynomial $P(s)$ of the closed-loop system is given as:

$$P(s) = A(s)D(s) + N(s)B(s) = \begin{pmatrix} \left(l_1 s^1\right)\cdot\left(s^2 + \left(\dfrac{2}{R\cdot C}\right)s + \dfrac{(1-\alpha)^2}{2\cdot L\cdot C}\right) + \\ + \left(\dfrac{(1-\alpha)}{L\cdot C}\right)\cdot\left(k_2 s^2 + k_1 s^1 + k_0\right) \end{pmatrix}. \tag{19}$$

Applying some mathematical manipulations, the characteristic polynomial $P(s)$ can be written as:

$$P(s)=\begin{pmatrix} l_1\cdot s^3+\left(\frac{(1-\alpha)}{L\cdot C}\cdot k_2+\frac{2.l_1}{R\cdot C}\right)\cdot s^2+\\ +\left(\frac{(1-\alpha)}{L\cdot C}\cdot k_1+\frac{(1-\alpha)^2}{2\cdot L\cdot C}\cdot l_1\right)\cdot s+\\ +\frac{(1-\alpha)}{L\cdot C}\cdot k_0. \end{pmatrix} \quad (20)$$

The target characteristic polynomial $P_t(s)$ is given as:

$$P_t(s)=a_0\left[\left(\sum_{i=2}^{3}\left(\prod_{j=1}^{i-1}\frac{1}{\gamma_{i-j}^{j}}\right)(\tau\cdot s)^i\right)+\tau\cdot s+1\right]. \quad (21)$$

Applying some mathematical manipulations and simplifications, the target characteristic polynomial $P_t(s)$ can be written as:

$$P_t(s)=\begin{pmatrix} \left(\frac{1}{\gamma_2^1\gamma_1^2}a_0\tau^3\right)\cdot s^3+\left(\frac{1}{\gamma_1^1}a_0\tau^2\right)\cdot s^2+\\ +(a_0\cdot\tau)\cdot s+a_0 \end{pmatrix}. \quad (22)$$

The time constant $\tau$ and $a_0$ are picked as follows for our application: $\tau = 0.001$ and $a_0 = 1$. The stability indices $\gamma_1$ and $\gamma_2$ are selected as $\gamma_i = [2.5, 2]$, $i = 1, 2$. In order to improve the system's performance, these parameters were picked from the Manabe's standard form.

Putting $P(s) = P_t(s)$, by identification between (20) and (22), the polynomials expressions can be written as:

$$\begin{cases} l_1=\frac{1}{\gamma_2^1\gamma_1^2}a_0\tau^3;\\ \frac{(1-\alpha)}{L\cdot C}k_2+\frac{2l_1}{R\cdot C}=\frac{1}{\gamma_1^1}a_0\tau^2;\\ \frac{(1-\alpha)}{L\cdot C}k_1+\frac{(1-\alpha)^2}{2\cdot L\cdot C}l_1=a_0\tau;\\ \frac{(1-\alpha)}{L\cdot C}k_0=a_0. \end{cases} \quad (23)$$

In matrix form ($AX = B$), the matrix equations of the polynomials expressions (23) are given as:

$$A=\begin{pmatrix} 0 & 0 & 0 & 1\\ \frac{(1-\alpha)}{L\cdot C} & 0 & 0 & \frac{2}{R\cdot C}\\ 0 & \frac{(1-\alpha)}{L\cdot C} & 0 & \frac{(1-\alpha)^2}{2\cdot L\cdot C}\\ 0 & 0 & \frac{(1-\alpha)}{L\cdot C} & 0 \end{pmatrix};$$

$$X=\begin{pmatrix} k_2\\ k_1\\ k_0\\ l_1 \end{pmatrix};\quad B=\begin{pmatrix} \frac{a_0\tau^3}{\gamma_2^1\gamma_1^2}\\ \frac{a_0\tau^2}{\gamma_1^1}\\ a_0\tau\\ a_0 \end{pmatrix},$$

where $X$ is the matrix of gains for estimating the PID controller parameters.

The previous design steps of the CDM-PID controller are programed in MATLAB editor. Achieved results are discussed in the following section.

**Results and discussion.** Simulation of the proposed two levels DC-DC boost-connected PV is validated through MATLAB environment. Table 1 displays the electrical parameters of the solar panel Solarex MSX-60.

Table 1

The electrical parameters of the solar panel Solarex MSX-60

| Parameter | Value |
|---|---|
| Maximum power $P_{max}$, W | 60 |
| Number of cells | 36 |
| Voltage at maximum power $V_{mpp}$, V | 17.1 |
| Current at maximum power $I_{mpp}$, A | 3.5 |
| Minimum power guaranteed, W | 58 |
| Short-circuit current $I_{cc}$, A | 3.8 |
| Open circuit voltage $V_{co}$, V | 21.1 |
| Temperature coefficient at $V_{co}$, mV/°C | –(80±10) |
| Temperature coefficient at $I_{cc}$, %/°C | (0.065±0.015) |
| Approximate effect of power temperature, %/°C | –(0.5±0.05) |

Figures 5,*a*,*b* illustrate the curves of PV panel characteristics, the current-voltage (*I-V*) characteristic and the power-voltage (*P-V*) characteristic, respectively.

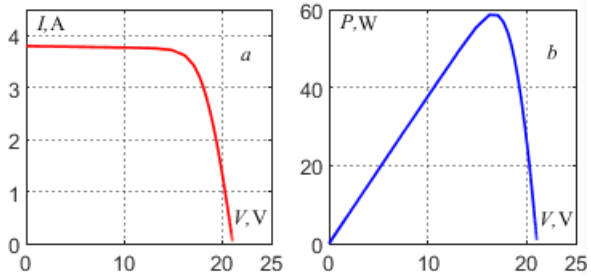


Fig. 5. Characteristics of a PV panel:
*a* – *I-V* characteristic; *b* – *P-V* characteristic

Figure 6 illustrates the impact of irradiance and temperature on the $I = f(V)$ and $P = f(V)$ characteristics.

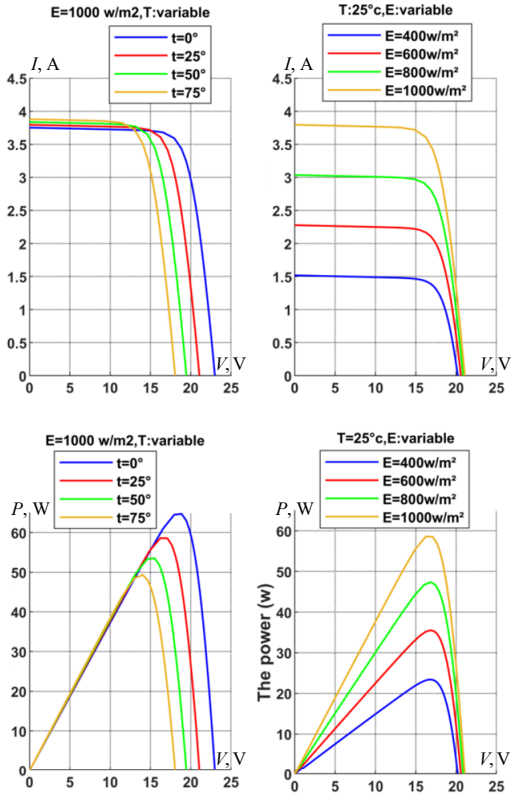


Fig. 6. *I-V* and *P-V* curves of the solar panel with various scenarios of temperature and irradiance values

To check the system through simulation, the parameters of the converter are given in Table 2.

Table 2
The electrical parameters of the converter

| Parameter | Value |
|---|---|
| Input voltage $V_s$, V | 30 |
| Switching frequency, kHz | 1 |
| Inductance $L$, mH | 800 |
| Capacitances $C_1$, $C_2$, $C_3$, μF | 220 |
| Resistance $R$, Ω | 1500 |
| Duty cycle $\alpha$ | 0.5 |

Figure 7 shows example of gate signal for the switch $S_1$ with $f = 1$ kHz and variable duty cycle $\alpha$. Figure 8 shows the input and output voltages of the two-level boost converter with duty cycle $\alpha = 0.5$. From Fig. 8 we note that the output voltage achieve a maximum value equal to 120 V with an input value equal to 30 V. Equation (9) confirm the obtained results.

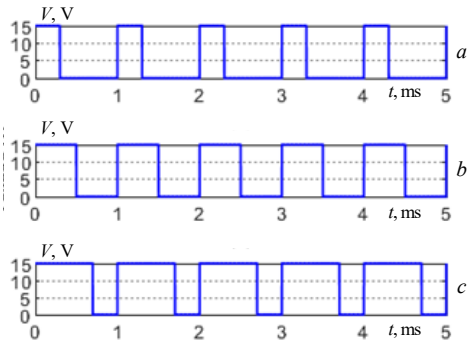


Fig. 7. Simulation example of gate signal for the switch $S_1$ with $f = 1$ kHz: $a$ – $\alpha = 30$ %; $b$ – $\alpha = 50$ %; $c$ – $\alpha = 70$ %.

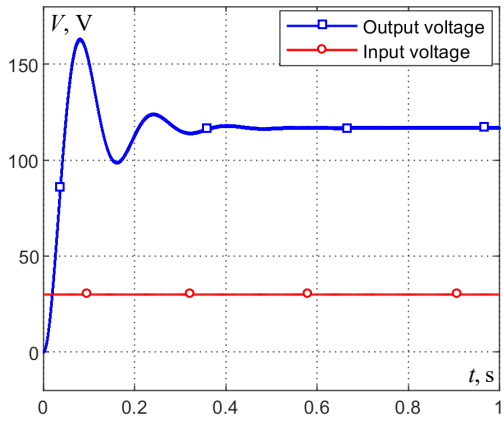


Fig. 8. Input and output voltages of the two-level boost converter with duty cycle $\alpha = 50$ %

Now, we will execute the programmed CDM-PID code in MATLAB editor. Solving the system gives the coefficients of the PID controller as: $k_p = 4.3997 \cdot 10^3$; $k_i = 4.4 \cdot 10^6$; $k_d = 1.7579$.

After achieving the PID controller parameters using the CDM, the next step is testing the system responses. Figure 9 illustrates the system's output with the CDM-PID controller in the scenario of variable reference. The reference was changed from 5 V to 20 V, and then to 10 V.

According to the achieved simulation results, it can be seen that the system output tracks the variable reference with a good accuracy and quickly, where the system output follows the reference path after varying its value; therefore, the PID based on CDM controller provides a good dynamic response to the system.

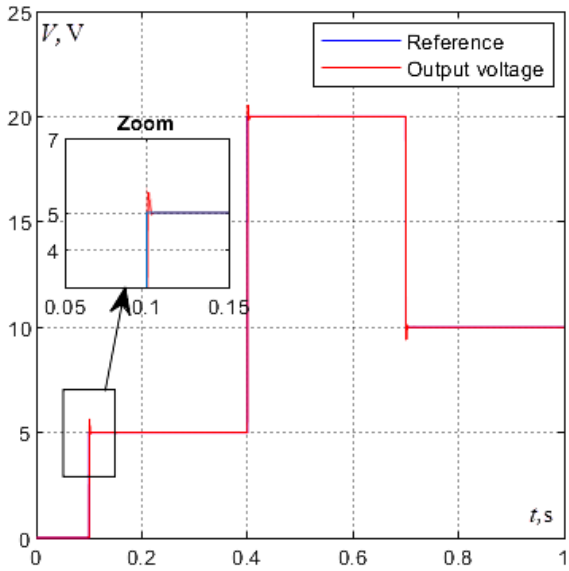


Fig. 9. System responses with the PID based on CDM controller in the case of variable reference

For testing the robustness of the PID-CDM controller, disturbance is injected in the closed-loop system. Figure 10 shows the block diagram of the closed-loop system when adding disturbance. The effects of the disturbances and their corresponding system responses are depicted in Fig. 11.

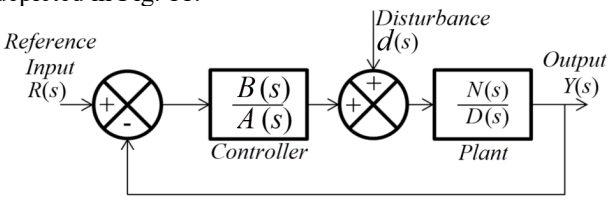


Fig. 10. Block diagram of the closed-loop system with disturbance

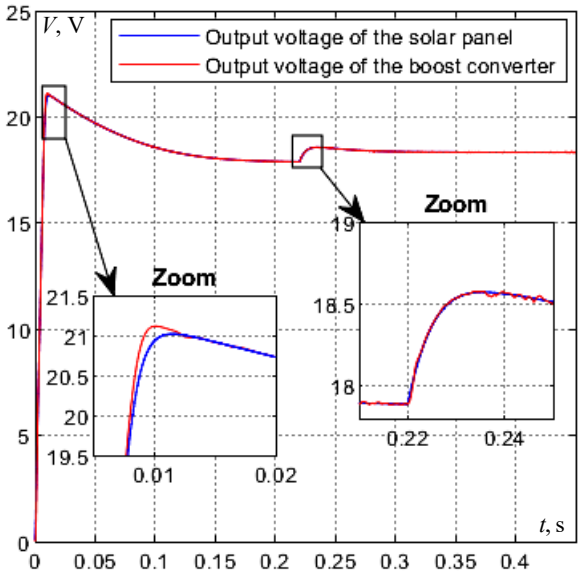


Fig. 11. System response with PID-CDM controller when adding disturbance

The curves in Fig. 11 demonstrate that the disturbances are rejected. The system responses return to the reference trajectory in the case of step disturbance.

According to the obtained simulation results, it can be seen that the PID-CDM controller provides good system responses and robust rejection of the disturbance.

**Experimental results.** To validate the achieved theoretical and simulation results, an experimental setup of the two-level boost converter with PV system has been constructed using one MOSFET switch, one inductance, three capacitors, three diode, one resistor as load, one DC power supply as PV panel, Arduino chip, oscilloscope, and PC with MATLAB/Simulink software. Figure 12 illustrates the experimental prototype of the proposed system.

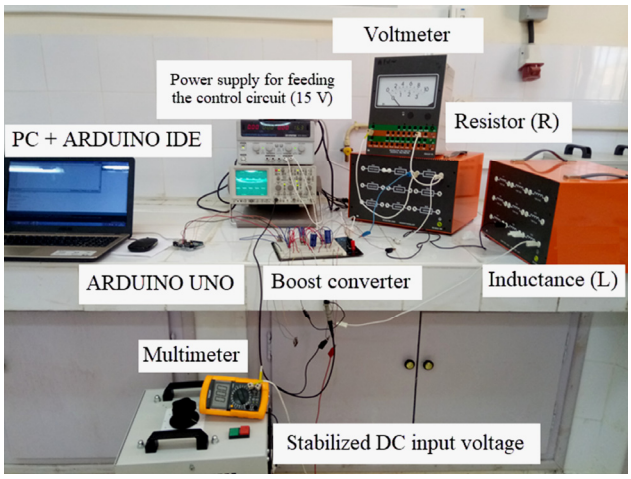


Fig. 12. Prototype of the two-level boost converter

Figure 13 demonstrates an experimental example of gate signal for the switch $S_1$ with switching frequency $f$ = 1 kHz and variable duty cycle: $a$ – $\alpha$ = 30 %, $b$ – $\alpha$ = 50 %, $c$ –$\alpha$ = 70 %, respectively.

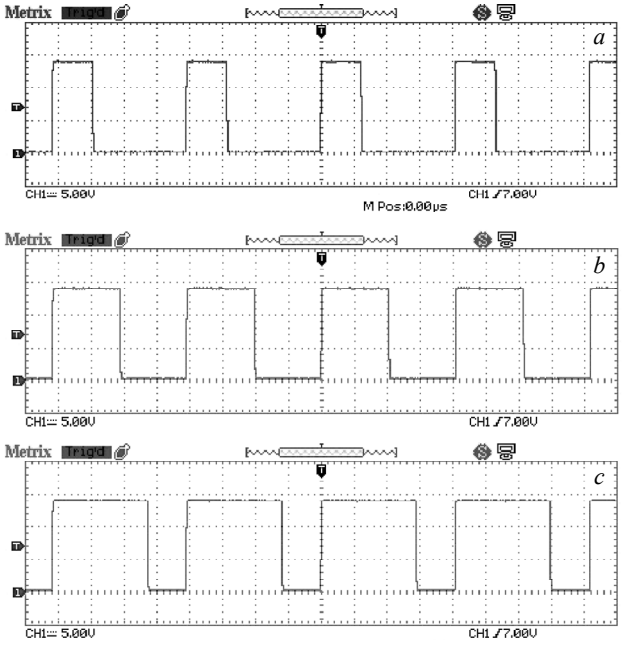


Fig. 13. Experimental example of gate signal for the switch $S_1$ with $f$ = 1 kHz and duty cycle $a$ – $\alpha$ = 30 %, $b$ – $\alpha$ = 50 %, $c$ – $\alpha$ = 70 %

Figure 14 shows the capacitors voltage and the output voltage of the two-level boost converter with duty cycle $\alpha$ = 0.5, and switching frequency $f$ = 1 kHz. From Fig. 14 we note that the output voltage $V_o$ achieve a maximum value equal to 120 V with an input value equal to 30 V.

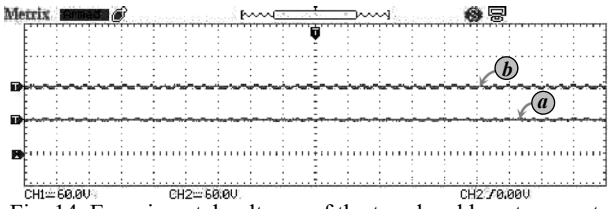


Fig. 14. Experimental voltages of the two-level boost converter with duty cycle $\alpha$ = 50 %: $a$ – the capacitors voltages; $b$ – the output voltage $V_o$

Figure 7 illustrates simulation example of gate signal for the switch $S_1$ with $f$ = 1 kHz and variable duty cycle using MATLAB/Simulink. Figure 13 illustrates the experimental gate signal for the switch $S_1$ using the experimental prototype. By comparison, the simulation results are matching closely the experimental one. Also, the simulation analyses of the converter output voltage $V_o$ is matching closely the experimental analyses as shown in Fig. 14. All the results were achieved using a simple and accurate design method.

**Conclusions.**

1. A mathematical model of a new system composed of coefficient diagram method based PID controller and two-level boost converter with photovoltaic system has been developed and investigated. The model allows to design the controller parameters based on the coefficient diagram method.

2. The two-level boost converter has been employed to extract the maximum power from the photovoltaic panel. coefficient diagram method based PID controller has been used to control the output voltage.

3. Simulation was done in MATLAB/Simulink software to verify the performance of the proposed system. In addition, an experimental evaluation was conducted using a low-cost Arduino board. The experimental results confirm that coefficient diagram method for controling multilevel boost converter is an effective and easy-to-apply technique.

4. As an extension to the work, it looks interesting to implement other methods to design the controller parameters, like the intelligent metaheuristic algorithms. Control the system with fuzzy logic controller, or neural network controller. Furthermore, other similar systems can be addressed, such as: feeding the multilevel boost converter with other renewable energies as the wind. The principal advantages of sustainable energies are to meet the increasing demand for electricity, particularly in the event of natural crises and international problems, to reduce air pollution and to limit global warming.

**Conflict of interest.** The authors declare that they have no conflicts of interest.

REFERENCES

*1.* Sai Thrinath B.V., Prabhu S., Meghya Nayak B. Power quality improvement by using photovoltaic based shunt active harmonic filter with Z-source inverter converter. *Electrical Engineering & Electromechanics*, 2022, no. 6, pp. 35-41. doi: https://doi.org/10.20998/2074-272X.2022.6.06.

*2.* Oumaymah E., Abdellah O., Omar B., Lhoussain E.B. NPC five level inverter using SVPWM for Grid-Connected Hybrid Wind-Photovoltaic Generation System. *Advances in Science, Technology and Engineering Systems Journal*, 2020, vol. 5, no. 6, pp. 981-987. doi: https://doi.org/10.25046/aj0506117.

*3.* Bekhoucha N., Mesbahi N., Bouchikha H., Heguig L., Chikha S. Model Predictive Control of Three-Level Shunt

Active Power Filter Connected to a Photovoltaic System. *2022 19th International Multi-Conference on Systems, Signals & Devices (SSD)*, 2022, pp. 128-133. doi: https://doi.org/10.1109/SSD54932.2022.9955660.
**4.** Maamar A.E.T., Helaimi M., Taleb R., Analysis, Simulation and Experimental Validation of High Frequency DC/AC Multilevel Inverter. *Przegląd Elektrotechniczny*, 2020, no. 8, pp. 16-19. doi: https://doi.org/10.15199/48.2020.08.03.
**5.** Nebti K., Lebied R. Fuzzy maximum power point tracking compared to sliding mode technique for photovoltaic systems based on DC-DC boost converter. *Electrical Engineering & Electromechanics*, 2021, no. 1, pp. 67-73. doi: https://doi.org/10.20998/2074-272X.2021.1.10.
**6.** Maamar A.E.T., Kermadi M., Helaimi M., Taleb R., Mekhilef S. An Improved Single-Phase Asymmetrical Multilevel Inverter Structure With Reduced Number of Switches and Higher Power Quality. *IEEE Transactions on Circuits and Systems II: Express Briefs*, 2021, vol. 68, no. 6, pp. 2092-2096. doi: https://doi.org/10.1109/TCSII.2020.3046186.
**7.** Benkahla M., Taleb R., Boudjema Z. A new robust control using adaptive fuzzy sliding mode control for a DFIG supplied by a 19-level inverter with less number of switches. *Electrical Engineering & Electromechanics*, 2018, no. 4, pp. 11-19. doi: https://doi.org/10.20998/2074-272X.2018.4.02.
**8.** Toubal Maamar A.E., Helaimi M., Taleb R., Kermadi M., Mekhilef S., Wahyudie A., Rawa M. Analysis and Small Signal Modeling of Five-Level Series Resonant Inverter. *IEEE Access*, 2021, no. 9, pp. 109384-109395. doi: https://doi.org/10.1109/ACCESS.2021.3102102.
**9.** Elamri O., Oukassi A., Toubal Maamar A.E., El Bahir L. Design and Simulation of a Power System Composed of Grid-tied Five-level Inverter with LCL Filter. *Electronics*, 2022, vol. 26, no. 1, pp. 17-25. doi: https://doi.org/10.53314/ELS2226017E.
**10.** Muthubalaji S., Devadasu G., Srinivasan S., Soundiraraj N. Development and validation of enhanced fuzzy logic controller and boost converter topologies for a single phase grid system. *Electrical Engineering & Electromechanics*, 2022, no. 5, pp. 60-66. doi: https://doi.org/10.20998/2074-272X.2022.5.10.
**11.** Chandramouli B., Vijayaprabhu A., Arun Prasad D., Kathiravan K., Udhayaraj N., Vijayasanthi M. Design of single switch-boosted voltage current suppressor converter for uninterrupted power supply using green resources integration. *Electrical Engineering & Electromechanics*, 2022, no. 5, pp. 31-35. doi: https://doi.org/10.20998/2074-272X.2022.5.05.
**12.** Romashko V.Y., Batrak L.M., Abakumova O.O. Step-up/step-down regulators in maximum power transmission mode. *Electrical Engineering & Electromechanics*, 2022, no. 2, pp. 18-22. doi: https://doi.org/10.20998/2074-272X.2022.2.03.
**13.** Ayat Y., Badoud A.E., Mekhilef S., Gassab S. Energy management based on a fuzzy controller of a photovoltaic/fuel cell/Li-ion battery/supercapacitor for unpredictable, fluctuating, high-dynamic three-phase AC load. *Electrical Engineering & Electromechanics*, 2023, no. 3, pp. 66-75. doi: https://doi.org/10.20998/2074-272X.2023.3.10.
**14.** Toubal Maamar A.E., Helaimi M., Taleb R., Kermadi M., Mekhilef S. A neural network-based selective harmonic elimination scheme for five-level inverter. *International Journal of Circuit Theory and Applications*, 2022, vol. 50, no. 1, pp. 298-316. doi: https://doi.org/10.1002/cta.3130.
**15.** Kumar R.S., Reddy C.S.R., Chandra B.M. Optimal performance assessment of intelligent controllers used in solar-powered electric vehicle. *Electrical Engineering & Electromechanics*, 2023, no. 2, pp. 20-26. doi: https://doi.org/10.20998/2074-272X.2023.2.04.
**16.** Anwar N., Hanif A., Ali M.U., Zafar A. Chaotic-based particle swarm optimization algorithm for optimal PID tuning in automatic voltage regulator systems. *Electrical Engineering & Electromechanics*, 2021, no. 1, pp. 50-59. doi: https://doi.org/10.20998/2074-272X.2021.1.08.
**17.** Manabe S. Coefficient Diagram Method. *IFAC Proceedings Volumes*, 1998, vol. 31, no. 21, pp. 211-222. doi: https://doi.org/10.1016/S1474-6670(17)41080-9.
**18.** Ikeda H. PID Controller Design Methods for Multi-Mass Resonance System. *PID Control for Industrial Processes*, 2018, pp. 187-207. doi: https://doi.org/10.5772/intechopen.74298.
**19.** Haouari F., Nourdine B., Boucherit M.S., Tadjine M. A Coefficient Diagram Method Controller with Backstepping Methodology for Robotic Manipulators. *Journal of Electrical Engineering*, 2015, vol. 66, no. 5, pp. 270-276. doi: https://doi.org/10.2478/jee-2015-0044.
**20.** Toubal Maamar A.E., Ladjouzi S., Taleb R., Kacimi Y. Détection et classification de défauts pour un GPV: Etude comparative entre la méthode de seuillage et réseaux de neurones. *Revue des Energies Renouvelables*, 2018, vol. 21, no. 1, pp. 45-53. (Fra).
**21.** Humada A.M., Hojabri M., Mekhilef S., Hamada H.M. Solar cell parameters extraction based on single and double-diode models: A review. *Renewable and Sustainable Energy Reviews*, 2016, vol. 56, pp. 494-509. doi: https://doi.org/10.1016/j.rser.2015.11.051.
**22.** Kermadi M., Berkouk E.M. Artificial intelligence-based maximum power point tracking controllers for Photovoltaic systems: Comparative study. *Renewable and Sustainable Energy Reviews*, 2017, vol. 69, pp. 369-386. doi: https://doi.org/10.1016/j.rser.2016.11.125.
**23.** Savitha P.B., Shashikala M.S., Puttabuddhi K.L. Modelling of Photovoltaic Cell/Module under Environmental Disturbances using MATLAB/Simulink. *International Journal of Engineering Trends and Technology*, 2014, vol. 9, no. 1, pp. 48-55. doi: https://doi.org/10.14445/22315381/IJETT-V9P210.
**24.** Tian H., Mancilla-david F., Ellis K., Jenkins P., Muljadi E. A Detailed Performance Model for Photovoltaic Systems. Preprint. *Solar Energy Journal*, 2012, 56 p.

*Received 20.05.2023*
*Accepted 15.07.2023*
*Published 02.01.2024*

*Kamel Latreche*[1]*, PhD Student,*
*Rachid Taleb*[2]*, Professor,*
*Abderrahim Bentaallah*[1]*, Professor,*
*Alla Eddine Toubal Maamar*[3]*, Assistant Professor,*
*M'hamed Helaimi*[2]*, Professor,*
*Fayçal Chabni*[4]*, Assistant Professor,*
[1] Electrical Engineering Department, Djillali Liabes University, Intelligent Control and Electrical Power Systems Laboratory (ICEPS), Sidi Bel Abbes, Algeria,
e-mail: ka.latreche02@gmail.com (Corresponding Author); bentaallah65@yahoo.fr
[2] Electrical Engineering Department,
Hassiba Benbouali University,
Laboratoire Génie Electrique et Energies Renouvelables (LGEER), Chlef, Algeria.
e-mail: rac.taleb@gmail.com; halimi1976@yahoo.fr
[3] Electrical Systems Engineering Department, Faculty of Technology, M'hamed Bougara University, Boumerdes, Algeria,
e-mail: allaeddine140dz@gmail.com
[4] Electronics Department,
Abdellah Morseli University Center, Tipaza, Algeria,
e-mail: fayssalc@gmail.com

*How to cite this article:*
Latreche K., Taleb R., Bentaallah A., Toubal Maamar A.E., Helaimi M., Chabni F. Design and experimental implementation of voltage control scheme using the coefficient diagram method based PID controller for two-level boost converter with photovoltaic system. *Electrical Engineering & Electromechanics*, 2024, no. 1, pp. 3-9. doi: https://doi.org/10.20998/2074-272X.2024.1.01